Optimization of the methacrylation of carboxymethylcellulose and use for the design of hydrogels and cryogels with controlled structure and properties

Lénaïc Soullard, Pierre-Alain Bayle, Christine Lancelon-Pin, Sébastien Rolere, Isabelle Texier, Bruno Jean, Guillaume Nonglaton

Optimization of the methacrylation of carboxymethylcellulose and use for the design of hydrogels and cryogels with controlled structure and properties

Lénaïc Soullard[a,b,c], Pierre-Alain Bayle[d], Christine Lancelon-Pin[c], Sébastien Rolere[a], Isabelle Texier[b], Bruno Jean[c] and Guillaume Nonglaton*[b]

*guillaume.nonglaton@cea.fr

[a] *Univ. Grenoble Alpes, CEA, LITEN, DTNM, Grenoble, France*

[b] *Univ. Grenoble Alpes, CEA, LETI, DTBS, Grenoble, France*

[c] *Univ. Grenoble Alpes, CNRS, CERMAV, Grenoble, France*

[d] *Univ. Grenoble Alpes, CEA, IRIG, MEM, Grenoble, France*

ABSTRACT

Carboxymethylcellulose (CMC) was functionalized using methacrylic anhydride (MA) to produce photo-crosslinkable methacrylated carboxymethylcellulose (mCMC). Optimization of the synthesis led to a wide range of mCMC samples with well-controlled degrees of methacrylation (DM) up to 76 ± 6 %, surpassing the literature data. Aqueous mCMC formulations with different DM and concentrations of mCMC were UV-cured to obtain hydrogels, which were transformed into cryogels after freeze-drying. An innovative ^{13}C CP-MAS solid-state NMR methodology was used to calculate the crosslinked methacrylate density in cryogels and thus in hydrogels. These values (from 4.3×10^{-3} to 1.3×10^{-2} mmol/cm^3) were correlated with both the DM and the mCMC concentration in formulations. These parameters were used to control the material microstructure and rheological properties. As a result, the swelling ratio of hydrated cryogels could be modulated for applications requiring high or low water absorption. Moreover, it was shown that the elastic moduli G' of the hydrated cryogels were superior to those of the original hydrogels, over the entire frequency range (0.1-10 Hz).

Keywords: *Carboxymethylcellulose, methacrylation, photo-crosslinking, hydrogel, cryogel*

Introduction

Polysaccharides such as hyaluronic acid, dextran, or cellulose, have been used for many years in biomedical applications due to their interesting features such as biocompatibility, biodegradability or biological properties (mucoadhesion, antimicrobial properties, etc.) (Rebelo, Fernandes, & Fangueiro 2017). These raw materials can eventually be chemically modified to improve their mechanical properties, to confer biological properties (specific cell targeting, biodegradability, etc.) (Luo et al. 2021) or defined shapes and porosities (Muir & Burdick 2020). For example, the methacrylation of these natural polymers can be used to form hydrogels by photo-crosslinking. The resulting materials are three-dimensional polymer networks with entrapped water, with potential applications in bone reconstruction (Poldervaart et al. 2017), tissue engineering (Chen et al. 2012), wound healing (Baier Leach et al. 2003), drug delivery (Matricardi et al. 2008) or 3D cell culture (García-Lizarribar et al. 2018). It is also possible to remove the entrapped water by freeze-drying to obtain cryogels (Darpentigny et al. 2020; Hossen et al. 2018), which are more stable and robust than hydrogels (Memic et al. 2020). These spongy materials can absorb a large amount of solvent thanks to their high porosity (Pacelli et al. 2021), which is interesting for the transport of nutrients or cells through scaffolds (Razavi, Qiao & Thakor 2019). Their robustness is also useful for bone tissue regeneration (Gu et al. 2020).

Although dextran and hyaluronic acid are the most studied polysaccharides for such applications (Dovedytis, Liu & Bartlett 2020), carboxymethylcellulose (CMC) is also of great interest for the elaboration of hydrogels by photo-crosslinking (Reeves et al. 2010). This cellulose derivative is biocompatible, water-soluble, and displays carboxylate and hydroxyl groups amenable to chemical functionalization (Rahman et al. 2021). One of the most studied reaction for the grafting of photo-crosslinkable methacrylate groups onto CMC consists of the condensation of the hydroxyl groups with methacrylic anhydride (MA) to yield methacrylated carboxymethylcellulose (mCMC) (García-Lizarribar et al. 2018, Hossen et al. 2018, Dutta, Samanta, & Dhara 2016). After photo-crosslinking, CMC hydrogels have been considered for biomedical applications such as cell encapsulation (Reza et Nicoll 2010), tissue engineering (Lin et al. 2016) or drug delivery (Dutta, Samanta, et Dhara 2016). mCMC cryogels have also been studied for their water absorption capacity (Hossen et al., 2018).

In order to benefit from tunable structures and properties (e.g. mechanical) of the CMC hydrogels and cryogels, which will allow targeting one or the other biomedical application, it is firstly of crucial importance to be able to control the degree of methacrylation (DM) of the mCMC, as already highlighted for other polymers such as methacrylated dextran (van Dijk-Wolthuis et al. 1997) and gelatin (Chen et al. 2012). However, in all previously reported studies, the DM of the mCMC never exceeded 60 % (Melilli et al., 2020), which limits the possible uses of such products. The influence of parameters such as the extent of methacrylate conversion and polymer concentration, which can also play a major role in the structural and mechanical properties of hydrogels and cryogels based on mCMC, have also been poorly investigated yet.

Herein, we report successful efforts to control the degree of methacrylation of mCMC samples and extend its range to values never achieved before. Beyond this optimization of the DM, we also investigated for the first time to the best of our knowledge the influence of the DM and concentration on the structural and physical properties of photo-crosslinked mCMC materials, either in the form of hydrogels or cryogels, and studied their

swelling behavior. Useful information were also obtained from the evaluation by solid-state NMR of the conversion ratio in photo-crosslinked mCMC samples (cryogels).

Materials and Methods

Materials

Sodium salt of CMC (NaCMC, reference BLANOSE 7LP EP, Ashland, France) with a weight-average molar mass (M_w) of 90.5 kg/mol and a degree of substitution (DS) of 0.7, was used as received. Methacrylic anhydride (MA) containing 2,000 ppm topanol A as inhibitor, 2-hydroxy-4'-(2-hydroxyethoxy)-2-methylpropiophenone (Irgacure 2959), anhydrous sodium hydroxide (NaOH) pellets and deuterium oxide (D_2O) were purchased from Sigma Aldrich (France).

Methacrylation of carboxymethylcellulose

The protocol was adapted from Melilli et al. (2020). NaCMC was solubilized at 2 wt% in deionized water at room temperature under stirring. MA was then added dropwise to the CMC solution. Different molar ratios between MA and CMC hydroxyl groups were used (namely 1.24, 2.48, 3.72 and 4.96) to study the effect of this parameter on the degree of methacrylation of the resulting mCMC samples. Homogenization during the reaction was performed by magnetic stirring at 700 rpm or by mechanical stirring at 2,000 rpm with a glass shaft anchor stirrer, to investigate the influence of the stirring method on the reaction. The reaction was continued for 24 h at room temperature. The pH of the medium was constantly adjusted to 8 with 10 M NaOH during the reaction. The resulting mixture was purified for a week by dialysis against deionized water using a cellulose mixed ester membrane (MWCO = 12-14 kg/mol; Roth, Germany). Finally, the mCMC product was freeze-dried for five days with a CHRIST Beta 2-8 LS plus lyophilizer (Martin Christ Gefriertrocknungsanlagen, Germany).

Hydrogel and cryogel preparations

The freeze-dried synthetised mCMC samples were dissolved at 2, 3 or 4 wt% in deionized water at 50 °C during 12h under magnetic stirring. The photoinitiator Irgacure 2959 was then added at room temperature with a constant molar ratio compared to the number of moles of methacrylate (MA) in solution (nPI/nMA = 0.55). Irgacure 2959 was chosen because it is water-soluble (0.5 wt% maximum), non-toxic, and absorbs at 365 nm (Tomal & Ortyl 2020). The formulations were treated for 15 min in an ultrasonic bath at 50 °C and then agitated with a multi-rotator PTR-35 (Grant, UK) at 6 rpm for 12 h at room temperature. 650 µL of each formulation was then placed in a PTFE circular mold of 15 mm diameter and 1 cm height and then insolated for 5 min under a UV-light source with a wavelength of 365 nm and an irradiance of 82 mW/cm² (Promaker V6000, Prodways, France). All resulting hydrogels had a thickness of 3.6 mm and a diameter of 15 mm. They were placed in an aluminum basket, filled with liquid nitrogen and freeze-dried overnight with the same lyophilizer to yield cryogels.

Characterization techniques

Nuclear magnetic resonance (NMR)

^{1}H NMR spectroscopy

^{1}H NMR spectroscopy was used to quantify the degree of methacrylation (DM) of the mCMC samples. 4.5 mg of mCMC was dissolved in 650 µL of D_2O at 50 °C for 12 h using a ThermoMixer C (Eppendorf, Germany). All ^{1}H NMR spectra were recorded on a Spectrospin 300 MHz spectrometer (Bruker, Germany) at 25 °C from 64 successive scans with a relaxation time D1 of 3 s.

^{13}C Non-Quaternary Suppression (NQS) and Cross-Polarization Magic-Angle Spinning (CP-MAS) solid state NMR spectroscopy

^{13}C NQS and CP-MAS solid-state NMR experiments were carried out to identify and quantify carbons before and after crosslinking of mCMC. ^{13}C CP-MAS solid-state NMR spectroscopy was also used to measure the crosslinking ratio of UV-cured cryogels. 80 mg of crosslinked mCMC cryogel was crushed and placed in a 3 mm diameter rotor. All ^{13}C NQS and CP-MAS solid-state NMR spectra were recorded on a Neo 500 MHz spectrometer (Bruker, Germany) operating at 125.8 MHz. The acquisition time was 28 ms and the sweep width was 37 kHz and at least 2,048 successive scans were recorded at 25 °C.

Fourier-transformed infrared (FTIR) spectroscopy

FTIR by attenuated total reflectance (ATR) was performed with a MIRacle 10 instrument (Shimadzu, Japon) to analyze the characteristic chemical bonds of CMC and mCMC samples. Absorbance spectra were acquired within the 4,000 – 550 cm^{-1} wavenumber range (64 scans, 4 cm^{-1} resolution).

Scanning electron microscopy (SEM)

SEM was used to investigate the cryogel morphology and measure the pore size distribution. Samples were fractured horizontally and pasted on metallic stubs with carbon cement, fractured and sputter-coated with Au/Pd. Secondary electron images were recorded with a FEI Quanta 250 (Thermo Fisher Scientific, US) scanning electron microscope equipped with a field emission gun operating at 2.5 kV. All pores were observed on the cutted surface. The pore size was determined by image treatment with ImageJ. Horizontal or vertical lines were drawn on each pore giving the average pore size. This procedure was performed on 25 pores per image and 4 images per sample. Pores whose walls were broken by the cutting method were not measured.

Swelling ratio and hydrogel mesh size calculation

Swelling tests were performed on cryogels. Measurements were made on 3 cryogels per condition. The samples were immersed in deionized water at room temperature and the cryogels transformed this way into hydrogels (or re-hydrated cryogels) were regularly weighed. These steps were repeated until mass equilibrium was reached to determine the swelling ratios (SR) according to Eq. (1).

$$SR = w_t/w_0 \quad (1)$$

where w_0 is the cryogel weight and w_t is the weight at measurement time t. Swelling ratios were averaged over measurements carried out on three different samples.

The hydrogel mesh size, ξ, was estimated from swelling tests, based on the previously described Flory-Rehner theory used by Baier Leach et al. (2003) and Lin et al. (2016). First, the mass ratio between the hydrogel and cryogel, Q_w, was calculated using Eq. (2):

$$Q_w = w_h/\mathrm{w}_0 \quad (2)$$

where w_h is the hydrogel weight and w_0 is the cryogel weight. The volumetric ratio, Q_v, between the hydrogel and the polymer volumes, was determined from Q_w using Eq. (3):

$$Q_v = 1 + \left(\frac{\rho_{mCMC}}{\rho_{water}}(Q_w - 1)\right) \quad (3)$$

where ρ_{mCMC} is the density of the considered dried mCMC measured by pycnometry, by analyzing pellets of each mCMC using an AccuPyc II 1340 pycnometer (Micromeritics, US) (Supplementary data - Table S1); ρ_{water} is the solvent density ($\rho_{water} = 1\ \mathrm{g.cm^{-3}}$). The average molecular weight between two crosslinking points ($\overline{\mathrm{M_c}}$) was calculated using a simplified version of the Flory-Rehner equation (4) demonstrated by Hoti et al. (2021):

$$\overline{M_c} = \frac{V_{water}\left[\left(\frac{w_H}{w_{hC}}\right)^{\frac{1}{3}} - \left(\frac{2}{f}\frac{w_H}{w_{hC}}\right)\right]}{-\left[ln\left(1-\frac{w_H}{w_{hC}}\right) + \frac{w_H}{w_{hC}} + \chi\left(\frac{w_H}{w_{hC}}\right)^2\right]} \quad (4)$$

where V_{water} is the molar volume of the solvent at room temperature (V_{water} = 18 mol.cm^{-3}), w_H is the hydrogel weight, w_{hC} is the weight of the hydrated cryogel at the maximum of swelling, χ is the Flory polymer-solvent interaction parameter and f is the functionality of the crosslinking, *i.e.* the maximum number of chemically linked polymer chains at a crosslinking point (f = 2.3 for CMC samples with DS = 0.7). Considering that CMC and mCMC have a similar structure, a value of 0.45 was used for χ, which corresponds to the CMC-water interaction parameter determined by Xia et al. (2013). The differences between CMC, mCMC and crosslinked mCMC were assumed to be negligible based on the work of Baier Leach et al. (2003) on hyaluronic acid (HA), methacrylate HA (mHA) and the crosslinked mHA.

The hydrogel mesh size, ξ was determined by Torres-Lugo and Peppas (1999) using Eq. (5):

$$\xi = \mathrm{Q_v^{\frac{1}{3}}}\left(\frac{\sqrt{\overline{\mathrm{M_c}}}}{\sqrt{\mathrm{M_w}}}\right)\sqrt{\overline{\mathrm{r_0}}^2} \quad (5)$$

where M_w is the molar mass of the mCMC, calculated depending on the DM, and $\overline{r_0}^2$ is the root-mean-square distance between two crosslinking points that can be linked to the molar mass M_n of the mCMC by Cleland (1970) using Eq. (6):

$$\sqrt{\overline{r_0}^2} = \sqrt{\frac{2C_n l^2}{M_r}}\sqrt{M_w} \quad (6)$$

where M_r is the molecular weight of the mCMC unit. C_n is the Flory characteristic ratio of CMC (11.5) determined by Picout & Ross-Murphy (2002) and l is the lengh of a virtual bond spanning a monosaccharide unit (0.545 nm) determined by Holtzer, Benoit & Doty (1954).

Finally, the hydrogel mesh size was calculated using Eq. (7):

$$\xi = \sqrt{\frac{2C_n l^2}{M_r}}\sqrt{\overline{M_c}}Q_v^{\frac{1}{3}} \quad (7)$$

Rheology measurements

The rheological properties of each hydrogel were measured at least on three different samples per hydrogel composition using a Netzsch Kinexus Pro+ parallel plates rheometer (Germany). Frequency sweep measurements were performed at a constant temperature (25 °C) from 0.1 to 10 Hz. According to preliminary amplitude sweep measurements, all tests were carried out in the linear viscoelastic region at 1 % strain. The gap between the plate and the mobile plane was set to 0.4 mm. Rheology measurements were also performed on hydrated cryogels at equilibrium swelling using the same procedure.

Results and discussion

Control and optimization of the methacrylation of CMC

Photo-crosslinkable methacrylate groups were successfully grafted onto CMC using the reaction between methacrylic anhydride (MA) and the polymer hydroxyl groups (Fig. 1a). In the literature, the reaction was only performed at low temperature (0 or 4 °C) (Reza & Nicoll 2010, Qian et al. 2014, Dutta et al. 2016, Melilli et al. 2020). However, no influence of temperature was observed in our study when comparing reactions performed at 0 °C or at room temperature (Supporting Information Fig. S1). Therefore, the reactions described below were more conveniently performed at room temperature and were fully optimized by varying protocol parameters.

All mCMC samples were characterized by FTIR spectroscopy, and the appearance of a carbonyl band at 1,705 cm^{-1} on the spectra of methacrylated samples when compared to the CMC spectrum (Supporting Information Fig. S2) qualitatively proved the success of the methacrylation (Supporting Information Fig. S2). Then, the samples were characterized by liquid ^1H NMR and compared to raw CMC (Fig. 1b) to determine the degree of methacrylation. According to the literature, protons of the CMC unit (H_{CMC}) are located in the bulk between 2.8 and 4.7 ppm (Kono et al. 2016), and account for 8.4 protons considering a DS of 0.7. For mCMC samples, three additional peaks corresponding to the vinyl (H_a: 6.0-6.4 ppm, H_b: 5.65-6.0 ppm) and methyl (H_c: 1.7 - 2.2 ppm) protons of the methacrylate groups were also found after purification, indicating that methacrylation occurred under our experimental conditions (Van Hove, Wilson & Benoit 2013). The deprotonation of hydroxyl groups is achieved by adding NaOH. The resulting hydroxide ion reacts with one of the carbons in the carbonyl group of MA, leading to the liberation

of methacrylic acid. CMC methacrylation should first preferentially occur on the remaining 30 % of C6 primary hydroxyl groups, which are more reactive (Fedorova et Rogovin 1963). Once all C6 hydroxyl groups are consumed, methacrylation will then occur on the C2 and C3 secondary hydroxyl groups. The reaction between the carboxylate group of CMC and MA is unlikely, as the carboxylate group is stabilized by mesomeric effects. Furthermore, mCMC remains water-soluble, proving the conservation of carboxylates. It is however difficult to verify these hypotheses by conventional characterizations. Nevertheless, recent advances in dynamic nuclear polarization NMR (DNP NMR) may allow determining the regioselectivity of the reaction as Berruyer et al. (2021) did with a substituted methylcellulose.

The degree of methacrylation of mCMC samples was calculated from the respective integrals of vinyl ($H_a + H_b$) and CMC (H_{CMC}) protons, according to Eq. (8).

$$\mathrm{DM}\ (\%) = \frac{H_a + H_b}{H_{CMC}} \times \frac{8.4}{2 \times 2.3} \times 100 \qquad (8)$$

The influence on the final DM of both the molar ratio between MA and CMC hydroxyl groups (MA/OH_{CMC}) and the agitation method was investigated. First, by increasing the MA/OH_{CMC} ratio from 0 to 4.96, a continuous increase in the integrals of all methacrylate peaks (H_a - H_c) was noticed (Fig. 1b), leading to a linear increase in the calculated DM (Fig. 1c; $R^2 > 0.94$). A maximum DM value of 76 ± 6 % was obtained for the mCMC prepared using a MA/OH_{CMC} ratio of 4.96 under mechanical stirring at 2,000 rpm, indicating that methacrylate groups successfully substituted 76 of the initial hydroxyl groups over 100 units. Such results therefore show a very easy and high degree of tunability of the DM by simply playing with the MA/OH ratio.

As for reactions performed using magnetic stirring at 700 rpm, a linear increase with the number of equivalents was observed. However, lower DM values were systematically obtained for the same molar ratio, which was attributed to a lower diffusion of MA in the solution. For example, for a MA/OH_{CMC} ratio of 4.96 under magnetic stirring, a DM of only 47 ± 4 % was obtained. The reaction was therefore found to be more efficient with mechanical stirring at 2,000 rpm.

It is worth noticing that the maximum DM obtained in this work is 76 ± 6 %, which is 16 percentage points higher than the maximum DM reported in the literature (DM = 60 %) by Melilli et al. (2020). According to the present results and since no plateau value was reached, it is quite likely that even higher DM values could be obtained by using a higher initial MA/OH_{CMC} ratio, but the influence of molar ratios larger than 4.96 was not studied here.

This methacrylation could be considered for other cellulosic derivatives. Methylcellulose has already been functionalized by MA and the development of the synthesis could be the same as the one presented here (Stalling, Akintoye, et Nicoll 2009; Gold et al. 2015). Similarly, hydroxypropyl cellulose has been functionalized by MA in N,N-dicyclohexylcardodiimide with pyridine instead of NaOH (A. Qi et al. 2014). The synthesis conditions described in this work could be adapted to this cellulose derivative. However, these conditions could not be suitable for cellulose acetate which is not water-soluble.

The mCMC samples discussed below were all synthesized using mechanical stirring, with initial MA/OH_{CMC} ratio of 1.24, 2.48 and 4.96 and had final DM values of 34 ± 4 % (sample A), 50 ± 5 % (sample B) and 76 ± 6 % (sample C), respectively.

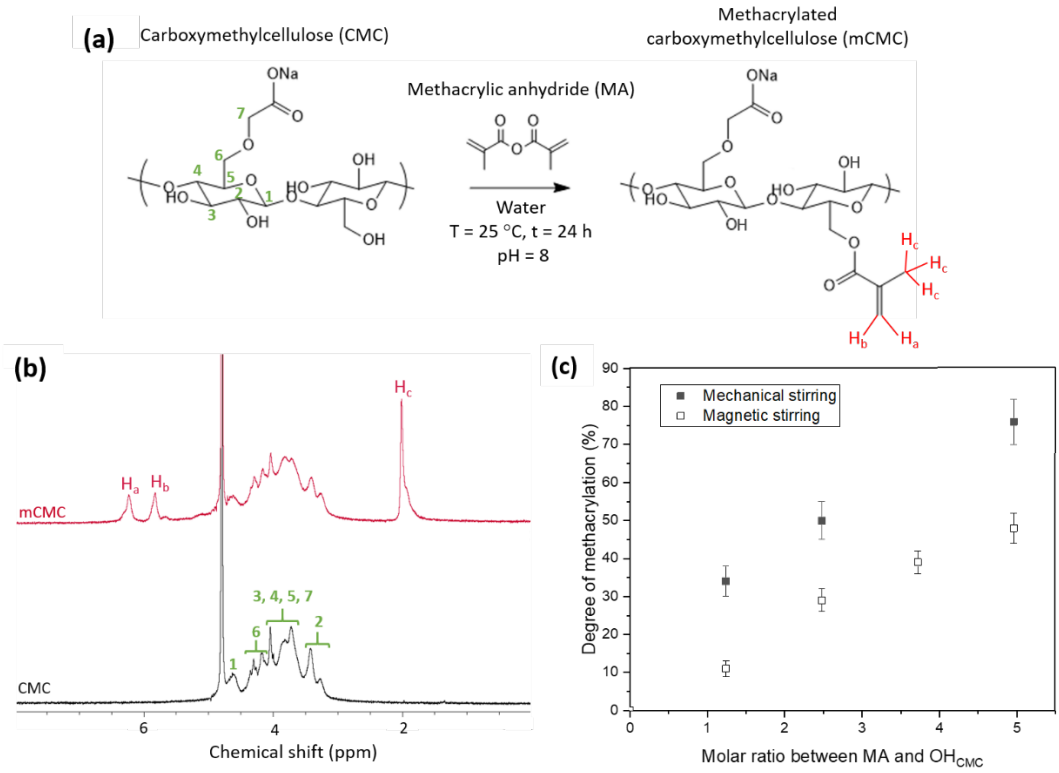

Fig. 1 (a) Scheme of the methacrylation of CMC with MA in water at 25 °C to yield mCMC. **(b)** ^{1}H NMR spectra for CMC in black and mCMC in red (2.48 eq, mechanical stirring, sample B). **(c)** Evolution of the degree of methacrylation with the molar ratio between MA and CMC hydroxyl groups for syntheses performed with mechanical and magnetic stirring. Error bars depend on the repetition of the synthesis (n= [1-3]) and the protons integration processing of the NMR spectra.

Hydrogels and cryogels characterization

The three mCMC samples (A-C) were then used to prepare eight photo-crosslinkable liquid formulations with mCMC concentrations between 2 and 4 wt% (Table 1). Due to its lower solubility in water, sample C (DM = 76 ± 6 %) was only used at 2 and 3 wt%. The influence of the UV insolation duration (30, 60 and 300 s) was then investigated by characterizing photo-crosslinked cryogel samples C3 using ^{13}C CP-MAS solid-state NMR (Supporting Information Fig. S2). The methacrylate conversion ratio calculated for these cryogels were 45 %, 54 % and 62 %, respectively, and rapidly reached a plateau value around 60 % (Supporting Information Fig. S4). Based on these results, the photo-crosslinking reaction was considered completed after 5 min, and this time was selected for the subsequently-described experiments.

Table 1 Composition of the photo-crosslinkable mCMC formulations, and structural properties of the corresponding hydrogels and cryogels.

Formulation	mCMC Sample	mCMC DM (%)	mCMC Concentration (wt%)	Cryogel Conversion ratio of methacrylates (CR) (%)	Cryogel Crosslinked methacrylate density (10^{-3} mmol/cm^3)[a]	Hydrogel Mesh size ξ (nm)
A2	A	34 ± 4	2	53 ± 2.0	4.3 ± 0.29	5.4 ± 1.6
A3			3	59 ± 2.0	6.4 ± 0.35	3.9 ± 1.2
A4			4	50 ± 2.0	8.1 ± 0.41	2.8 ± 0.96
B2	B	50 ± 5	2	58 ± 2.0	6.6 ± 0.39	4.2 ± 1.0
B3			3	54 ± 2.0	9.1 ± 0.50	2.8 ± 0.50
B4			4	53 ± 2.0	12 ± 0.65	0.79 ± 0.27
C2	C	76 ± 6	2	62 ± 2.0	9.9 ± 0.62	1.3 ± 0.38
C3			3	54 ± 2.0	13 ± 0.95	0.56 ± 0.14

[a] $Crosslinked\ methacrylate\ density = \frac{n_{meth}(mmol)\times CR}{100\times V_{cryogel}\,(cm^3)}$

Determination of the conversion ratio in photo-crosslinked mCMC

The methacrylate conversion ratio (CR) of all 8 cryogels was investigated by NMR spectroscopy. First, the ^{13}C CP-MAS spectra of the mCMC samples before crosslinking were used to attribute the signals of the different carbons, as already detailed (H. Qi et al. 2009). The heterocyclic carbons ($C_{2\text{-}5}$) were found between 55 and 90 ppm, while the anomeric carbon was found at 104 ppm (Fig. 2a). The signals at 168 and 176 ppm were attributed to the carbonyl of the methacrylate (C_9) and carboxylate (C_8) groups, respectively. (Capitani et al. 2000) showed that the raw unmethacrylated CMC only has a carbonyl signal at 176 ppm, in good accordance with this attribution. Finally, the signals at 18, 123 and 133 ppm were respectively attributed to the methyl carbon (C_{12}) and to both vinyl carbons ($C_{10\text{-}11}$) of the methacrylate group (Fig. 2a). A few differences were observed in the ^{13}C CP-MAS and NQS spectra of photo-crosslinked samples and attributed using sample C3 spectra (Fig. 2b and Supporting Information Fig. S3). During the UV insolation, the methacrylates of the C3 sample were progressively converted by vinyl polymerization, leading to a progressive decrease of carbons $C_{9\text{-}12}$ signal intensities. Simultaneously, the apparition of new carbon signals was observed and attributed to the crosslinking points formed by vinyl conversion: $C_{9'}$ (163 ppm), $C_{10'}$ (46 ppm), $C_{11'}$ (115 ppm) and $C_{12'}$ (28 ppm).

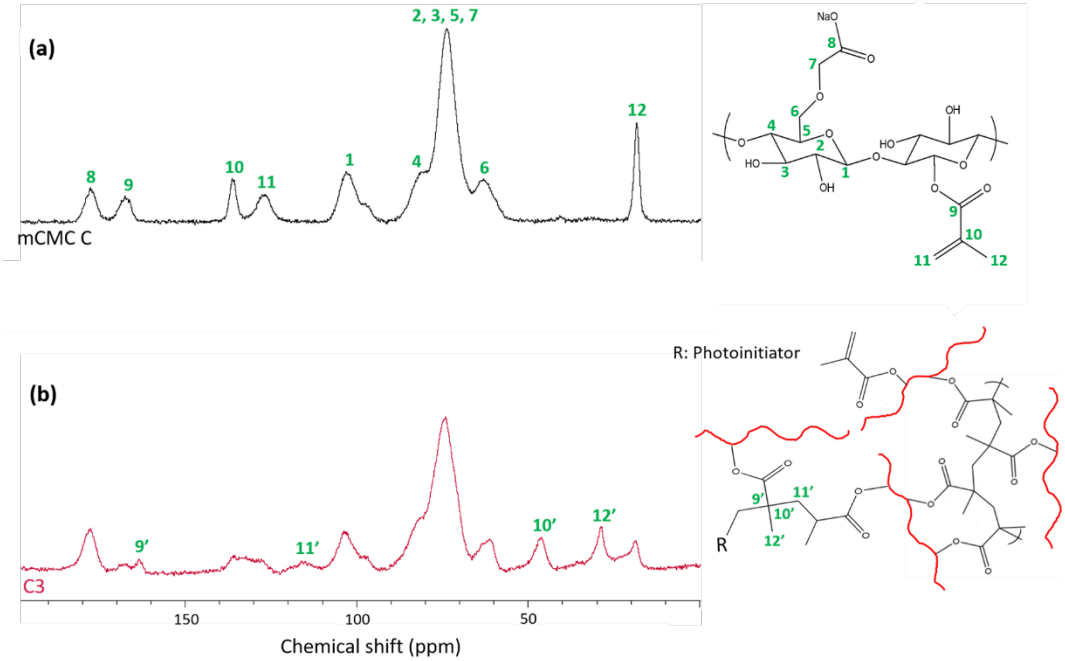

Fig. 2 ^{13}C CPMAS solid-state NMR spectra of **(a)** C mCMC sample (DM = 76 %) and **(b)** C3 cryogel.

The conversion ratio of methacrylates in the cryogel samples was then calculated by integrating the area of the C12' carbon peak from the C12 of the crosslinked mCMC, normalized by the anomeric carbon 1, which remained constant during crosslinking. Two carbons of Irgacure 2959 were also integrated at the same chemical shift (24 ppm). However, considering a constant molar ratio between the photoinitiator and the methacrylate groups (0.55), the Irgacure contribution does not modifiy the calculation of CR. The CR was therefore calculated with Eq. (9):

$$CR = \frac{A(C_{12'})}{A(C_{12}) + A(C_{12'})} \quad (9)$$

where $A(C_{12'})$ and $A(C_{12})$ correspond to the integrals of the $C_{12'}$ (28 ppm) and C_{12} (18 ppm) carbon signals of crosslinked mCMC, respectively.

Finally, the CR of methacrylates was calculated for all cryogels to determine its dependence with the initial degree of methacrylation (DM) and concentration of the mCMC in the formulations. Table 1 summarizes the extracted values that lie between 50 ± 2 % and 62 ± 2 %. It is very interesting to note that the mCMC concentration negatively impacted the final CR while the DM had little influence (Table 1). Indeed, the CR did not change significantly with increasing DM for the same initial concentration, while, on the other hand, for the same DM, the higher the concentration, the lower the CR. Considering that the volume of all cryogels was constant and equal to 0.64 cm^3, it was possible to calculate the density of crosslinked methacrylates in mmol/cm^3 from the DM and CR values (Table 1). Interestingly, the crosslinked methacrylate density increased linearly with the DM at a constant concentration (R^2 > 0.99; Fig. 3a), as well as with the concentration for a constant DM (R^2 > 0.98; Fig. 3b). The hydrogel crosslink density can thus be controlled over a significant range (3-fold increase between the lowest and highest densities) by modulating the initial DM of the considered mCMC, but also the mCMC concentration in the photo-crosslinkable formulation.

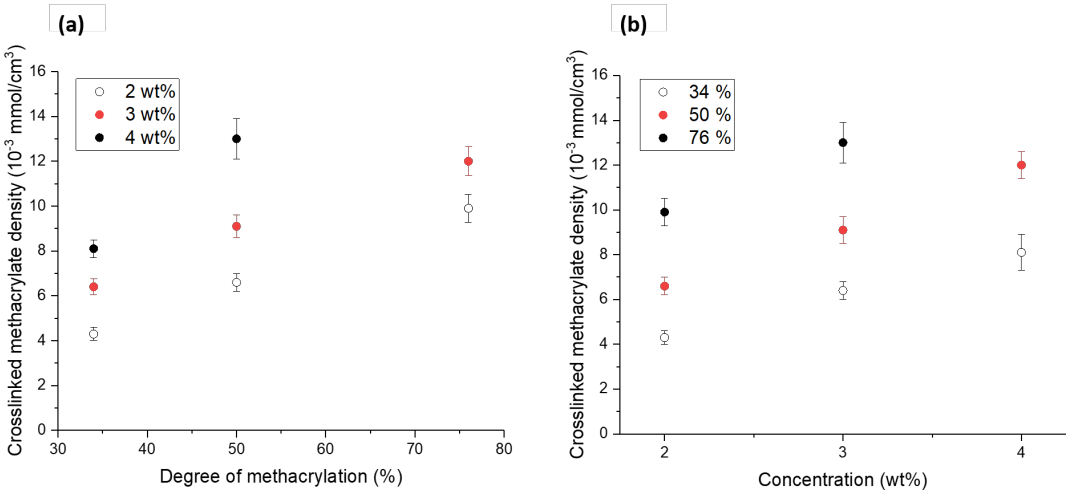

345

346 **Fig. 3** Density of crosslinked methacrylates according to **(a)** mCMC DM for a given concentration,
347 and **(b)** mCMC concentration for a given DM.

348 *Relationship between swelling and hydrogel and cryogel structure*

349 Water swelling ratios (SR) reflecting the capacity of cryogels to absorb and retain water
350 without breaking were measured. A swelling equilibrium was achieved in less than 10
351 hours for all cryogels (Supporting Information Fig. S5). Interestingly, the final swelling ratio
352 decreased with increasing concentration, with A2, A3 and A4 cryogels absorbing 81, 66
353 and 45 times more water than their initial mass after 48 h at room temperature,
354 respectively. Similarly, the swelling ratio decreased with increasing DM. For example,
355 swelling ratios of 81, 62 and 37 were obtained for the cryogels A2 (DM = 34 %), B2 (DM =
356 50 %) and C2 (DM = 76 %), respectively. The same trends were observed between the
357 swelling ratio and the crosslinked methacrylate density (Fig. 4a). When the crosslinked
358 methacrylate density in the cryogel increased, the network became denser and less
359 stretchable, and thus absorbed less water. The hydrated cryogel swelling ratios were then
360 compared to the water content of initial hydrogels (Fig. 4b). All cryogels absorbed more
361 water than that contained in the hydrogels, as the swelling was conducted to its maximum
362 capacity for the hydrated cryogels, whereas the equilibrium was probably not reached for
363 the initial hydrogels. Interestingly, differences in the swelling ratio between the two
364 materials were observed depending on the sample. For example, hydrated cryogels A2
365 with the lowest crosslink density was twice as heavy as the initial hydrogel A2, whereas
366 the most crosslinked cryogel B4 absorbed only 7 % more water than the initial hydrogel
367 B4 had. This could be explained by the freezing, which causes the polymer chains to
368 aggregate (Cassanelli, Norton, et Mills 2018). The swelling ratio at equilibrium strongly
369 depends on the intrinsic capacity of the polymer chains to absorb water (Ganji,
370 Vasheghani-Farahani, et Vasheghani-Farahani 2010). In the case of cryogels, the collapsed
371 polymer chains were held together by hydrogen bonds, making it more difficult for water
372 to hydrate them. This phenomenon became even more significant when mCMC
373 concentration increased, which could involve enlargement of the size of the pore walls as
374 observed by Cassanelli et al. (2018) with gellan gum cryogels. Finally, the water absorption
375 capacity of cryogels also appeared to depend on the free methacrylate density
376 (Supporting Information Fig. S6), since methacrylates are hydrophobic. The possibility to
377 finely tune the swelling capacity of hydrated cryogels makes it possible to consider several
378 types of medical applications. Indeed, it has been reported that the higher the water

content of hydrogels, the more they provide a functional environment for cells. Such a property would be beneficial for applications such as drug delivery (Chang et al. 2010) or wound healing (Kanikireddy et al. 2020; Uzun 2018). Moreover, higher water content allows for better biodegradability (Capanema et al. 2018; Chang et al. 2010). However, for other applications such as bone repair, a lower swelling ratio is recommended (Bai et al. 2018).

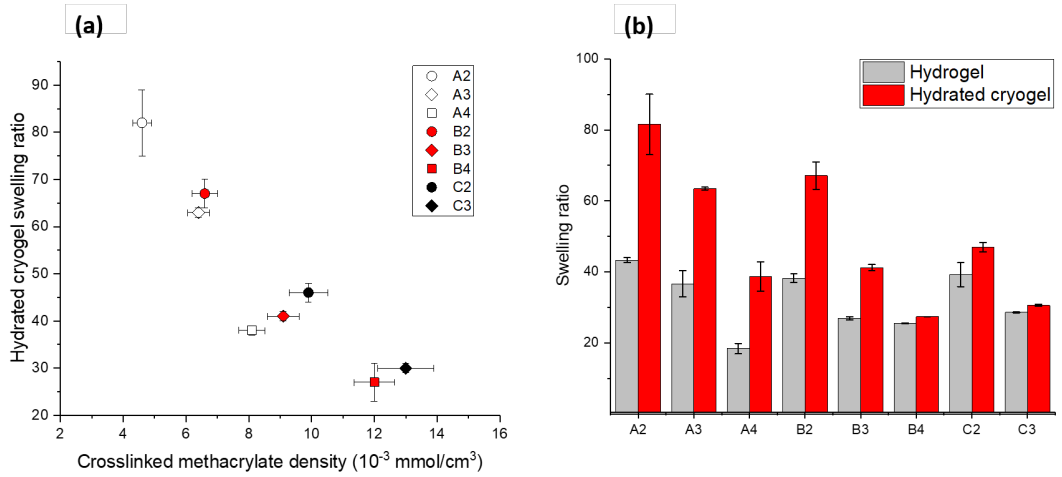

Fig 4 (a) Influence of the density of crosslinked methacrylates in cryogel samples on the swelling ratio of the hydrated cryogel after 48h. **(b)** Comparison of hydrogel water content and hydrated cryogel swelling ratio at equilibrium. Error bars are standard deviations for 3 different samples per formulation.

The density of crosslinked methacrylates also had an influence on the material structure. The hydrogel mesh size, representing the distance between two crosslinks, was evaluated using the Flory-Rehner theory for each formulation (Eq. 7). As expected, the mesh size decreased as the concentration and DM of mCMC increased (Table 1). The more methacrylate groups in the formulation, the more crosslinks and the smaller the mesh size. However, these results did not lead to significant variations in the cryogel pore sizes determined by SEM (Fig. 5, Supporting Information Fig. S7) as the most crosslinked sample (B4) had an average pore size of 13.9 ± 5.3 µm and the less crosslinked sample (A2) displayed an average pore size of 18.9 ± 6.5 µm. The variations would rather be reflected in the thickness of the walls constituting the pores (Plieva et al. 2005). In fact, the pore size and direction in the cryogels happen to be predominantly controlled by the freeze-drying process, and not directly by the material crosslink density. The influence of the freeze-drying process is currently under investigation. Regarding the size of the pores, they are too small for applications such as bone repair, for which pores around 200 µm are required to allow osteoblasts to penetrate the network (Abbasi et al. 2020; Sindhu, Prasanth, et Thakur 2014). To overcome this issue, it could be possible to shape grids by 3D printing with an adequate porosity. However, the range of pore size we could reach would be able to allow neovascularization or fibroblast growth (Annabi et al. 2010).

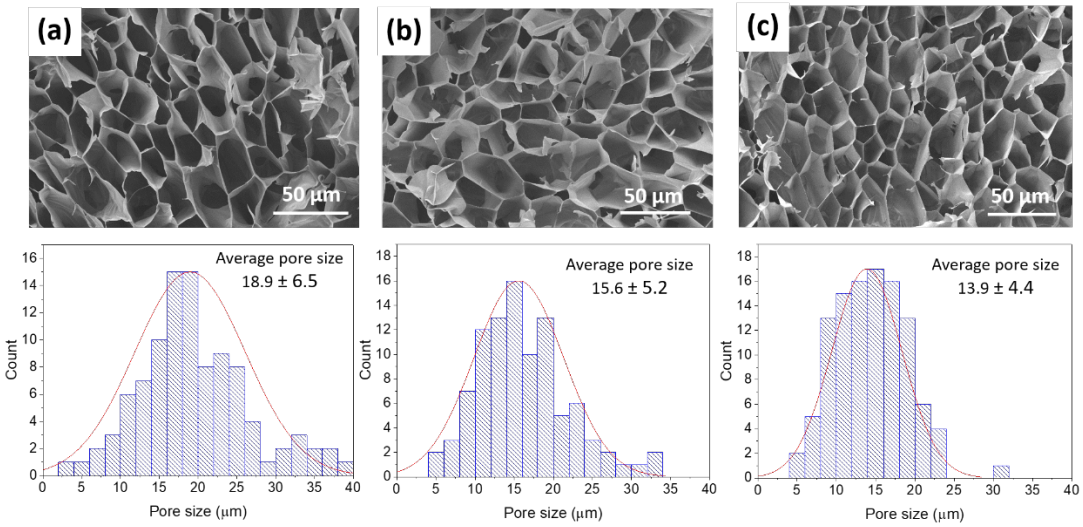

Fig. 5 SEM images displaying the cryogel morphologies and corresponding pore size distributions for **(a)** A2, **(b)** B2 and **(c)** C2. The average pore size was determined after around 25 measurements on 4 images per sample. Pores whose walls were broken by the cutting section method were not taken into account.

Rheological behavior

The impact of the crosslink density on the hydrogel mechanical properties was investigated by rheology. The evolution of the elastic modulus, G', viscous modulus, G'' and $\tan(\delta) = \frac{G''}{G'}$ were first compared for A2 and B4, the hydrogels bounding the range of rheological properties (Supporting Information Fig. S8). Over the entire frequency range (0.1 to 10 Hz) at 1 % strain and at 25 °C, G' is always superior to G'', which evidenced the solid behavior of the gels. Moreover, the same behavior was observed for all the hydrogels, irrespective of the formulation. Finally, the elastic and viscous moduli of hydrogels and hydrated cryogels maintained the same order as a function of DM and mCMC concentration in the formulations (Supporting Information Fig. S9). Consequently, the comparison of the solid rheological properties of the materials was performed by considering G' at 1 Hz. The same study could be done with G'' for the viscous behavior.

For hydrogels, G'(f) of the initial hydrogels increased with mCMC concentration (Fig. 6a). At 1 Hz, hydrogel G'(1 Hz) values of 1.8 ± 0.50, 3.5 ± 0.90 and 8.0 ± 0.40 kPa were measured for B2, B3 and B4, respectively. However, there was no significant trend observed with the DM. The same trend was observed with mCMC concentration for the hydrated cryogels (Fig. 6b). Hydrated cryogel G'(1 Hz) values of 8.6 ± 2.2, 13.1 ± 0.8 and 16.7 ± 1.7 kPa were measured for B2, B3 and B4, respectively. At 1 Hz, the ratio of elastic moduli (G'(hydrated cryogel)/G'(initial hydrogel) was superior to 1 for each formulation. Noticeably, even if they contain more water, the elastic moduli of the hydrated cryogels were significantly higher than those of the initial hydrogels. This ratio also decreased as the mCMC concentration increased. While at 2 wt% mCMC, the G' ratio increased with decreasing DM, no significant G' ratio evolution with DM was observed at 3 wt% and 4 wt% (Fig. 6c).

Such a difference in the rheological properties could be due to the liquid nitrogen-freezing step before freeze-drying. As observed in the SEM images along the cross-section

(Supporting Information Fig. S10), cryogel pores were oriented along the freezing axis (from the bottom to the top) after freeze-drying, whereas they could be randomly oriented in the hydrogels. It is conceivable that this orientation implies a stronger network organization in the cryogel than in the initial hydrogel. Indeed, cryogel swelling did not affect the variation of the elastic modulus G' of hydrated cryogels as a function of DM and mCMC concentration compared to hydrogels (Fig. 6a,b). The elastic moduli of both materials increased with mCMC concentration and did not show significant variation with DM. However, the less crosslinked methacrylate density in the formulation, the more water the initial hydrogel contained (Fig. 4b). It is possible that upon freezing the pore orientation and network organization is partly governed by the quantity of water in the initial hydrogel. In other words, the formed crystals could be larger in the presence of larger amounts of water. The microstructure could have deformed more easily and become more robust upon freeze-drying when more water was entrapped in the initial hydrogel. Moreover, the freezing process collapses the chains and can strengthen the structure of the 3D network. Indeed, the G' ratio decreased with the hydrogel water content (Fig. 6d). For B2, B3 and B4, G' ratios were 4.7 ± 0.10, 3.8 ± 0.61 and 2.1 ± 0.10 for a hydrogel water content of 38 ± 1.2, 28 ± 0.43 and 24 ± 0.010, respectively (Fig. 6d).

Finally, our results evidence that the elastic modulus G' of both initial hydrogels and hydrated cryogels can be tuned by varying the mCMC concentration, rather than the DM. Depending on the material targeted application, specific DM and concentration can be selected to achieve suitable microstructure and mechanical properties. As an example, hydrogels are generally mechanically brittle for bone repair applications (Bai et al. 2018; Sindhu, Prasanth, et Thakur 2014). It is shown here that it is possible to increase the viscoelasticity of hydrogels without increasing the amount of water in the hydrogel, as in the case of the B4 sample. However, the obtained elastic moduli are too low for skeletal tissues. On the other hand, they could be considered for use as extracellular matrix (ECM) or for soft tissue repair, such as lungs or brain (Chaudhuri et al. 2020).

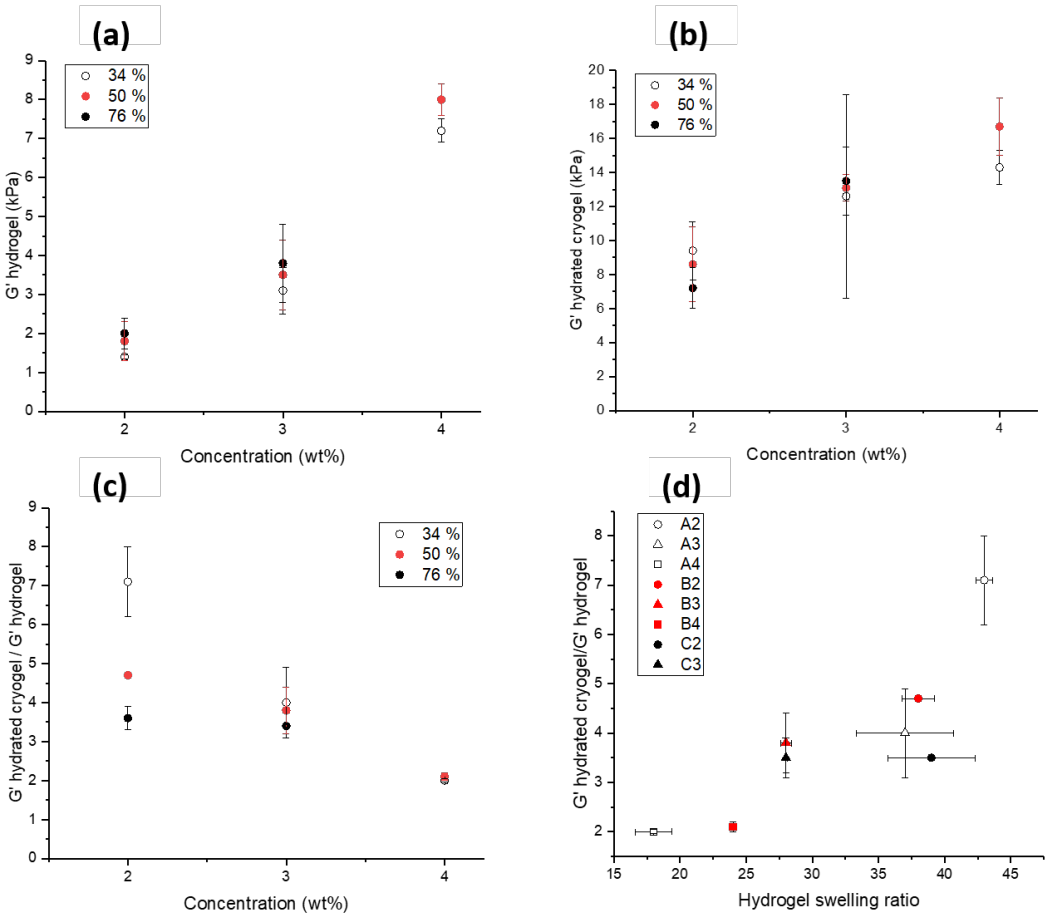

Fig 6 (a) Evolution of the elastic moduli G' of the initial hydrogels (at 1 Hz, 1% strain and 25 °C) versus the mCMC concentration in each formulation. **(b)** Evolution of the elastic moduli G' of the hydrated cryogels (at 1 Hz, 1% strain and 25 °C) versus the mCMC concentration in each formulation. **(c)** Ratios of the elastic moduli of hydrated cryogels over that of the corresponding initial hydrogels versus mCMC concentration. **(d)** Evolution of the ratios of the elastic moduli of hydrated cryogels over that of the corresponding hydrogels versus hydrogel swelling ratio. Error bars come from the standard deviation of three independent measurements.

4. Conclusion

In this study, the reaction between carboxymethylcellulose and methacrylic anhydride was first investigated to produce photo-crosslinkable methacrylated carboxymethylcellulose. By controlling the synthesis parameters, a wide range of mCMC samples with degrees of methacrylation ranging between 0 and 76 ± 6 % were obtained. Eight aqueous formulations with different DM and concentrations of mCMC were used to prepare UV-cured hydrogels, which were subsequently transformed into cryogels by freeze-drying. A new ^{13}C solid-state NMR method was used to measure the methacrylate conversion ratio (CR, from 50 to 62 %) and deduce the density of crosslinked methacrylates (from 4.3×10^{-3} to 1.3×10^{-2} mmol/cm^3) of the final cryogels, which was found to be correlated with both DM and initial concentration of the mCMC formulation. Furthermore, correlations between the density of crosslinked methacrylate and the swelling ratio of cryogels on the one hand, and the microstructure on the other hand, were demonstrated. In addition, these results help to explain the evolution of the elastic moduli of hydrogels and hydrated cryogels, which depended mainly on the initial

concentration of mCMC in the formulation. Furthermore, the difference between the two elastic moduli depended on the quantity of water in the initial hydrogel and the crosslinked methacrylate density. In conclusion, we highlighted the possibility of fine-tuning the microstructure (crosslinked methacrylate density; mesh size between 0.56 and 5.4 nm) as well as the cryogel swelling ratio (25-80) and rheological properties (2-8 kPa for hydrogels, 4.5 - 17 kPa for swollen cryogels) of UV-cured mCMC hydrogels and cryogels, by controlling the methacrylation conditions of a commercial CMC. According to the selected properties, these crosslinked mCMC hydrogels and cryogels could serve different purposes in biomedicine, such as 3D scaffolds for soft tissue regeneration, or cell encapsulation. Additionally, photo-crosslinkable mCMC could be easily shaped by 3D printing technics to obtain complex 3D-printed artefacts. Finally, these materials could also be considered in fields such as agriculture, food and textile where porous materials are generally used to absorb solvents, dyes, water or liquids harmful to the analyzed environment (Rahman et al. 2021).

ACKNOWLEDGEMENTS

The authors acknowledge the NanoBio chemistry platform (ICMG UAR 2607) for granting access to the electron microscopy facilities. The authors also acknowledge Ashland for kindly offering carboxymethylcellulose.

Author contribution All authors contributed to the study conception and design. Material preparation, data collection and analysis were performed by Lénaïc Soullard, Sébastien Rolere, Bruno Jean, Isabelle Texier, Guillaume Nonglaton, Pierre-Alain Bayle and Christine Lancelon-Pin. The first draft of the manuscript was written by Lénaïc Soullard and all authors commented on previous versions of the manuscript. All authors read and approved the final manuscript.

Funding Financial support from the cross cutting CEA program 'Matériaux et Procédés' is gratefully acknowledged (CelluloMed project). The authors acknowledge the Agence Nationale de la Recherche for financial support through the LabEx ARCANE program (ANR-11-LABX-0003-01) and the Graduate School of Chemistry, Biology and Health of University Grenoble Alpes CBH-EUR-GS (ANR-17-EURE-0003) and Glyco@Alps.

Availability of data and material Additional information regarding this manuscript can be found free of charge in the supporting information.

Declarations

Conflict of interest The authors have no conflicts of interest to declare.

Ethical approval All authors have read and understood the ''Ethical Responsibilities of Authors'' in the journal's ''Submission Guidelines'', including the passage on screening for plagiarism with computer software.

Consent for publication All authors have fully read, agreed, and approved the final version of the manuscript which has been submitted for possible publication.

References

Abbasi, Naghmeh, Stephen Hamlet, Robert M. Love, et Nam-Trung Nguyen. 2020. « Porous Scaffolds for Bone Regeneration ». *Journal of Science: Advanced Materials and Devices* 5 (1): 1-9. https://doi.org/10.1016/j.jsamd.2020.01.007.

Annabi, Nasim, Jason W. Nichol, Xia Zhong, Chengdong Ji, Sandeep Koshy, Ali Khademhosseini, et Fariba Dehghani. 2010. « Controlling the Porosity and Microarchitecture of Hydrogels for Tissue Engineering ». *Tissue Engineering Part B: Reviews* 16 (4): 371-83. https://doi.org/10.1089/ten.teb.2009.0639.

Bai, Xin, Mingzhu Gao, Sahla Syed, Jerry Zhuang, Xiaoyang Xu, et Xue-Qing Zhang. 2018. « Bioactive Hydrogels for Bone Regeneration ». *Bioactive Materials* 3 (4): 401-17. https://doi.org/10.1016/j.bioactmat.2018.05.006.

Baier Leach, Jennie, Kathryn A. Bivens, Charles W. Patrick Jr., et Christine E. Schmidt. 2003. « Photocrosslinked Hyaluronic Acid Hydrogels: Natural, Biodegradable Tissue Engineering Scaffolds ». *Biotechnology and Bioengineering* 82 (5): 578-89. https://doi.org/10.1002/bit.10605.

Berruyer, Pierrick, Martin Gericke, Pinelopi Moutzouri, Dörthe Jakobi, Michel Bardet, Leif Karlson, Staffan Schantz, Thomas Heinze, et Lyndon Emsley. 2021. « Advanced Characterization of Regioselectively Substituted Methylcellulose Model Compounds by DNP Enhanced Solid-State NMR Spectroscopy ». *Carbohydrate Polymers* 262 (juin): 117944. https://doi.org/10.1016/j.carbpol.2021.117944.

Capanema, Nádia S.V., Alexandra A.P. Mansur, Anderson C. de Jesus, Sandhra M. Carvalho, Luiz C. de Oliveira, et Herman S. Mansur. 2018. « Superabsorbent Crosslinked Carboxymethyl Cellulose-PEG Hydrogels for Potential Wound Dressing Applications ». *International Journal of Biological Macromolecules* 106 (janvier): 1218-34. https://doi.org/10.1016/j.ijbiomac.2017.08.124.

Capitani, Donatella, Matteo Alessandro Del Nobile, Giuseppe Mensitieri, Alessandro Sannino, et Anna Laura Segre. 2000. « ^{13}C Solid-State NMR Determination of Cross-Linking Degree in Superabsorbing Cellulose-Based Networks ». *Macromolecules* 33 (2): 430-37. https://doi.org/10.1021/ma9914117.

Cassanelli, Mattia, Ian Norton, et Tom Mills. 2018. « Role of Gellan Gum Microstructure in Freeze Drying and Rehydration Mechanisms ». *Food Hydrocolloids* 75 (février): 51-61. https://doi.org/10.1016/j.foodhyd.2017.09.013.

Chang, Chunyu, Bo Duan, Jie Cai, et Lina Zhang. 2010. « Superabsorbent Hydrogels Based on Cellulose for Smart Swelling and Controllable Delivery ». *European Polymer Journal* 46 (1): 92-100. https://doi.org/10.1016/j.eurpolymj.2009.04.033.

Chaudhuri, Ovijit, Justin Cooper-White, Paul A. Janmey, David J. Mooney, et Vivek B. Shenoy. 2020. « Effects of Extracellular Matrix Viscoelasticity on Cellular Behaviour ». *Nature* 584 (7822): 535-46. https://doi.org/10.1038/s41586-020-2612-2.

Chen, Ying-Chieh, Ruei-Zeng Lin, Hao Qi, Yunzhi Yang, Hojae Bae, Juan M. Melero-Martin, et Ali Khademhosseini. 2012. « Functional Human Vascular Network Generated in Photocrosslinkable Gelatin Methacrylate Hydrogels ». *Advanced Functional Materials* 22 (10): 2027-39. https://doi.org/10.1002/adfm.201101662.

Cleland, Robert L. 1970. « Ionic Polysaccharides. IV. Free-Rotation Dimensions for Disaccharide Polymers. Comparison with Experiment for Hyaluronic Acid ». *Biopolymers* 9 (7): 811-24. https://doi.org/10.1002/bip.1970.360090707.

Darpentigny, Clémentine, Sonia Molina-Boisseau, Guillaume Nonglaton, Julien Bras, et Bruno Jean. 2020. « Ice-Templated Freeze-Dried Cryogels from Tunicate Cellulose Nanocrystals with High Specific Surface Area and Anisotropic

578 Morphological and Mechanical Properties ». *Cellulose* 27 (1): 233-47.
579 https://doi.org/10.1007/s10570-019-02772-8.
580 Dijk-Wolthuis, W. N. E. van, J. A. M. Hoogeboom, M. J. van Steenbergen, S. K. Y. Tsang,
581 et W. E. Hennink. 1997. « Degradation and Release Behavior of Dextran-Based
582 Hydrogels ». *Macromolecules* 30 (16): 4639-45.
583 https://doi.org/10.1021/ma9704018.
584 Dovedytis, Matthew, Zhuo Jie Liu, et Samuel Bartlett. 2020. « Hyaluronic Acid and Its
585 Biomedical Applications: A Review ». *Engineered Regeneration* 1: 102-13.
586 https://doi.org/10.1016/j.engreg.2020.10.001.
587 Dutta, Sujan, Pousali Samanta, et Dibakar Dhara. 2016. « Temperature, PH and Redox
588 Responsive Cellulose Based Hydrogels for Protein Delivery ». *International*
589 *Journal of Biological Macromolecules* 87 (juin): 92-100.
590 https://doi.org/10.1016/j.ijbiomac.2016.02.042.
591 Fedorova, A.F., et Z.A. Rogovin. 1963. « A Study of the Relative Reactivity of the Hydroxyl
592 Groups of Cellulose in Esterification in an Acidic Medium ». *Polymer Science*
593 *U.S.S.R.* 4 (5): 1189-94. https://doi.org/10.1016/0032-3950(63)90350-2.
594 Fernández-Garibay, Xiomara, María A Ortega, Estefanía Cerro-Herreros, Jordi Comelles,
595 Elena Martínez, Rubén Artero, Juan M Fernández-Costa, et Javier Ramón-Azcón.
596 2021. « Bioengineered in Vitro 3D Model of Myotonic Dystrophy Type 1 Human
597 Skeletal Muscle ». *Biofabrication* 13 (3): 035035. https://doi.org/10.1088/1758-
598 5090/abf6ae.
599 Ganji, Fariba, Samira Vasheghani-Farahani, et Ebrahim Vasheghani-Farahani. 2010.
600 « Theoretical Description of Hydrogel Swelling: A Review ». *Iranian Polymer*
601 *Journal* 5 (19): 375-98.
602 García-Lizarribar, Andrea, Xiomara Fernández-Garibay, Ferran Velasco-Mallorquí, Albert
603 G. Castaño, Josep Samitier, et Javier Ramon-Azcon. 2018. « Composite
604 Biomaterials as Long-Lasting Scaffolds for 3D Bioprinting of Highly Aligned
605 Muscle Tissue ». *Macromolecular Bioscience* 18 (10): 1800167.
606 https://doi.org/10.1002/mabi.201800167.
607 Gold, Gittel T., Devika M. Varma, Peter J. Taub, et Steven B. Nicoll. 2015. « Development
608 of Crosslinked Methylcellulose Hydrogels for Soft Tissue Augmentation Using an
609 Ammonium Persulfate-Ascorbic Acid Redox System ». *Carbohydrate Polymers*
610 134 (décembre): 497-507. https://doi.org/10.1016/j.carbpol.2015.07.101.
611 Gu, Lihua, Yifan Zhang, Liwen Zhang, Yiqian Huang, Dawei Zuo, Qing Cai, et Xiaoping
612 Yang. 2020. « Comparative Study of Gelatin Cryogels Reinforced with
613 Hydroxyapatites with Different Morphologies and Interfacial Bonding ».
614 *Biomedical Materials* 15 (3): 035012. https://doi.org/10.1088/1748-
615 605X/ab7388.
616 Holtzer, Alfred M., Henri Benoit, et Paul Doty. 1954. « The Molecular Configuration and
617 Hydrodynamic Behavior of Cellulose Trinitrate ». *The Journal of Physical*
618 *Chemistry* 58 (8): 624-34. https://doi.org/10.1021/j150518a009.
619 Hossen, Muhammad R., Nayereh Dadoo, David G. Holomakoff, Aimee Co, William M.
620 Gramlich, et Michael D. Mason. 2018. « Wet Stable and Mechanically Robust
621 Cellulose Nanofibrils (CNF) Based Hydrogel ». *Polymer* 151 (août): 231-41.
622 https://doi.org/10.1016/j.polymer.2018.07.016.
623 Hoti, Gjylije, Fabrizio Caldera, Claudio Cecone, Alberto Rubin Pedrazzo, Anastasia
624 Anceschi, Silvia Lucia Appleton, Yousef Khazaei Monfared, et Francesco Trotta.
625 2021. « Effect of the Cross-Linking Density on the Swelling and Rheological
626 Behavior of Ester-Bridged β-Cyclodextrin Nanosponges ». *Materials* 14 (3): 478.
627 https://doi.org/10.3390/ma14030478.
628 Kanikireddy, Vimala, Kokkarachedu Varaprasad, Tippabattini Jayaramudu,
629 Chandrasekaran Karthikeyan, et Rotimi Sadiku. 2020. « Carboxymethyl
630 Cellulose-Based Materials for Infection Control and Wound Healing: A Review ».

International Journal of Biological Macromolecules 164 (décembre): 963-75. https://doi.org/10.1016/j.ijbiomac.2020.07.160.

Kono, Hiroyuki, Kazuhiro Oshima, Hisaho Hashimoto, Yuuichi Shimizu, et Kenji Tajima. 2016. « NMR Characterization of Sodium Carboxymethyl Cellulose: Substituent Distribution and Mole Fraction of Monomers in the Polymer Chains ». *Carbohydrate Polymers* 146 (août): 1-9. https://doi.org/10.1016/j.carbpol.2016.03.021.

Lin, Huizi A., Michelle S. Gupta, Devika M. Varma, M. Lane Gilchrist, et Steven B. Nicoll. 2016. « Lower Crosslinking Density Enhances Functional Nucleus Pulposus-like Matrix Elaboration by Human Mesenchymal Stem Cells in Carboxymethylcellulose Hydrogels: Crosslinking Density Impacts HMSC Chondrogenesis ». *Journal of Biomedical Materials Research Part A* 104 (1): 165-77. https://doi.org/10.1002/jbm.a.35552.

Luo, Moucheng, Xinyu Zhang, Jun Wu, et Jinmin Zhao. 2021. « Modifications of Polysaccharide-Based Biomaterials under Structure-Property Relationship for Biomedical Applications ». *Carbohydrate Polymers* 266 (août): 118097. https://doi.org/10.1016/j.carbpol.2021.118097.

Matricardi, Pietro, Marilena Pontoriero, Tommasina Coviello, Maria Antonietta Casadei, et Franco Alhaique. 2008. « In Situ Cross-Linkable Novel Alginate-Dextran Methacrylate IPN Hydrogels for Biomedical Applications: Mechanical Characterization and Drug Delivery Properties ». *Biomacromolecules* 9 (7): 2014-20. https://doi.org/10.1021/bm800252c.

Melilli, Giuseppe, Irene Carmagnola, Chiara Tonda-Turo, Fabrizio Pirri, Gianluca Ciardelli, Marco Sangermano, Minna Hakkarainen, et Annalisa Chiappone. 2020. « DLP 3D Printing Meets Lignocellulosic Biopolymers: Carboxymethyl Cellulose Inks for 3D Biocompatible Hydrogels ». *Polymers* 12 (8): 1655. https://doi.org/10.3390/polym12081655.

Memic, Adnan, Mahboobeh Rezaeeyazdi, Pierre Villard, Zachary J. Rogers, Tuerdimaimaiti Abudula, Thibault Colombani, et Sidi A. Bencherif. 2020. « Effect of Polymer Concentration on Autoclaved Cryogel Properties ». *Macromolecular Materials and Engineering* 305 (5): 1900824. https://doi.org/10.1002/mame.201900824.

Meyvis, Tom, Stefaan De Smedt, Barbara Stubbe, Wim Hennink, et Joseph Demeester. s. d. « On the Release of Proteins from Degrading Dextran Methacrylate Hydrogels and the Correlation with the Rheologic Properties of the Hydrogels », 7.

Michelle T. Poldervaart, Birgit Goversen, Mylene de Ruijter, Anna Abbadessa, Ferry P. W. Melchels, F. Cumhur Öner, Wouter J. A. Dhert, Tina Vermonden, et Jacqueline Alblas. 2017. « 3D Bioprinting of Methacrylated Hyaluronic Acid (MeHA) Hydrogel with Intrinsic Osteogenicity ». Édité par Masaya Yamamoto. *PLOS ONE* 12 (6): e0177628. https://doi.org/10.1371/journal.pone.0177628.

Muir, Victoria G., et Jason A. Burdick. 2020. « Chemically Modified Biopolymers for the Formation of Biomedical Hydrogels ». *Chemical Reviews*, décembre, acs.chemrev.0c00923. https://doi.org/10.1021/acs.chemrev.0c00923.

Pacelli, Settimio, Laura Di Muzio, Patrizia Paolicelli, Valeria Fortunati, Stefania Petralito, Jordan Trilli, et Maria Antonietta Casadei. 2021. « Dextran-Polyethylene Glycol Cryogels as Spongy Scaffolds for Drug Delivery ». *International Journal of Biological Macromolecules* 166 (janvier): 1292-1300. https://doi.org/10.1016/j.ijbiomac.2020.10.273.

Picout, David R, et Simon B Ross-Murphy. 2002. « On the Chain FLexibility of Arabinoxylans and Other B-(1 □4) Polysaccharides ». *Carbohydrate Research*, 4.

Plieva, Fatima M, Malin Karlsson, Maria-Rosa Aguilar, David Gomez, Sergey Mikhalovsky, et Igor Yu Galaev'. 2005. « Pore Structure in Supermacroporous Polyacrylamide Based Cryogels », 7.
Qi, Aisha, Siew Pei Hoo, James Friend, Leslie Yeo, Zhilian Yue, et Peggy P. Y. Chan. 2014. « Hydroxypropyl Cellulose Methacrylate as a Photo-Patternable and Biodegradable Hybrid Paper Substrate for Cell Culture and Other Bioapplications ». *Advanced Healthcare Materials* 3 (4): 543-54. https://doi.org/10.1002/adhm.201300155.
Qi, Haisong, Tim Liebert, Frank Meister, et Thomas Heinze. 2009. « Homogenous Carboxymethylation of Cellulose in the NaOH/Urea Aqueous Solution ». *Reactive and Functional Polymers* 69 (10): 779-84. https://doi.org/10.1016/j.reactfunctpolym.2009.06.007.
Qian, Hanqing, Xin Wang, Kangjun Yuan, Chen Xie, Wei Wu, Xiqun Jiang, et Lijiang Hu. 2014. « Delivery of Doxorubicin in Vitro and in Vivo Using Bio-Reductive Cellulose Nanogels ». *Biomater. Sci.* 2 (2): 220-32. https://doi.org/10.1039/C3BM60176E.
Rahman, Md. Saifur, Md. Saif Hasan, Ashis Sutradhar Nitai, Sunghyun Nam, Aneek Krishna Karmakar, Md. Shameem Ahsan, Muhammad J. A. Shiddiky, et Mohammad Boshir Ahmed. 2021. « Recent Developments of Carboxymethyl Cellulose ». *Polymers* 13 (8): 1345. https://doi.org/10.3390/polym13081345.
Razavi, Mehdi, Yang Qiao, et Avnesh S. Thakor. 2019. « Three-dimensional Cryogels for Biomedical Applications ». *Journal of Biomedical Materials Research Part A* 107 (12): 2736-55. https://doi.org/10.1002/jbm.a.36777.
Rebelo, Rita, Margarida Fernandes, et Raul Fangueiro. 2017. « Biopolymers in Medical Implants: A Brief Review ». *Procedia Engineering* 200: 236-43. https://doi.org/10.1016/j.proeng.2017.07.034.
Reeves, Robert, Andreia Ribeiro, Leonard Lombardo, Richard Boyer, et Jennie B. Leach. 2010. « Synthesis and Characterization of Carboxymethylcellulose-Methacrylate Hydrogel Cell Scaffolds ». *Polymers* 2 (3): 252-64. https://doi.org/10.3390/polym2030252.
Reza, Anna T., et Steven B. Nicoll. 2010. « Characterization of Novel Photocrosslinked Carboxymethylcellulose Hydrogels for Encapsulation of Nucleus Pulposus Cells ». *Acta Biomaterialia* 6 (1): 179-86. https://doi.org/10.1016/j.actbio.2009.06.004.
Sindhu, Karthika Ammini, Raghavan Prasanth, et Vijay Kumar Thakur. 2014. « Medical Applications of Cellulose and Its Derivatives: Present and Future ». In *Nanocellulose Polymer Nanocomposites*, édité par Vijay Kumar Thakur, 437-77. Hoboken, NJ, USA: John Wiley & Sons, Inc. https://doi.org/10.1002/9781118872246.ch16.
Sk, Md Moniruzzaman, Prativa Das, Amit Panwar, et Lay Poh Tan. 2021. « Synthesis and Characterization of Site Selective Photo-Crosslinkable Glycidyl Methacrylate Functionalized Gelatin-Based 3D Hydrogel Scaffold for Liver Tissue Engineering ». *Materials Science and Engineering: C* 123 (avril): 111694. https://doi.org/10.1016/j.msec.2020.111694.
Stalling, Simone S., Sunday O. Akintoye, et Steven B. Nicoll. 2009. « Development of Photocrosslinked Methylcellulose Hydrogels for Soft Tissue Reconstruction ». *Acta Biomaterialia* 5 (6): 1911-18. https://doi.org/10.1016/j.actbio.2009.02.020.
Tomal, Wiktoria, et Joanna Ortyl. 2020. « Water-Soluble Photoinitiators in Biomedical Applications ». *Polymers* 12 (5): 1073. https://doi.org/10.3390/polym12051073.
Uzun, Muhammet. 2018. « A Review of Wound Management Materials ». *Journal of Textile Engineering & Fashion Technology* 4 (1). https://doi.org/10.15406/jteft.2018.04.00121.
Van Hove, Amy H., Brandon D. Wilson, et Danielle S. W. Benoit. 2013. « Microwave-Assisted Functionalization of Poly(Ethylene Glycol) and On-Resin Peptides for

735 Use in Chain Polymerizations and Hydrogel Formation ». *Journal of Visualized*
736 *Experiments*, n° 80 (octobre): 50890. https://doi.org/10.3791/50890.
737 Xia, Zhiyong, Marcia Patchan, Jeffrey Maranchi, Jennifer Elisseeff, et Morgana Trexler.
738 2013. « Determination of Crosslinking Density of Hydrogels Prepared from
739 Microcrystalline Cellulose ». *Journal of Applied Polymer Science* 127 (6):
740 4537-41. https://doi.org/10.1002/app.38052.
741